PCCP

PAPER

View Article Online
View Journal | View Issue

Cite this: *Phys. Chem. Chem. Phys.*, 2017, **19**, 24667

Hydrophobic fluorine mediated switching of the hydrogen bonding site as well as orientation of water molecules in the aqueous mixture of monofluoroethanol: IR, molecular dynamics and quantum chemical studies†

Saptarsi Mondal, Biswajit Biswas, Tonima Nandy and Prashant Chandra Singh *

The local structures between water–water, alcohol–water and alcohol–alcohol have been investigated for aqueous mixtures of ethanol (ETH) and monofluoroethanol (MFE) by the deconvolution of IR bands in the OH stretching region, molecular dynamics simulation and quantum chemical calculations. It has been found that the addition of a small amount of ETH into the aqueous medium increases the strength of the hydrogen bonds between water molecules. In an aqueous mixture of MFE, the substitution of a single fluorine induces a change in the orientation as well as the hydrogen bonding site of water molecules from the oxygen to the fluorine terminal of MFE. The switching of the hydrogen bonding site of water in the aqueous mixture of MFE results in comparatively strong hydrogen bonds between MFE and water molecules as well as less clustering of water molecules, unlike the case of the aqueous mixture of ETH. These findings about the modification of a hydrogen bond network by the hydrophobic fluorine group probably make fluorinated molecules useful for pharmaceutical as well as biological applications.

Received 11th July 2017,
Accepted 21st August 2017

DOI: 10.1039/c7cp04663d

rsc.li/pccp

Introduction

Biological systems contain many molecules having both hydrophobic as well as hydrophilic groups and these molecules interact with water in different manners.[1–4] Intermolecular interactions such as hydrogen bonding between water and these molecules control the functionality of various important biological processes.[5,6] Aqueous mixtures of aliphatic alcohols like ethanol (ETH) are one of the important representatives of this class of systems.[3,7,8] Several experimental as well as simulation studies have been performed to understand the different physical, chemical and molecular level information about aqueous mixtures of ETH.[9–14]

Substitution of a single hydrogen with fluorine alters the molecular properties significantly.[15–19] Indeed, fluorocarbon groups have been used to design many non-canonical amino acids which stabilize proteins more effectively than unsubstituted amino acids.[20–23] Fluorinated molecules have been used for diverse applications such as reaction media,[3,24–27] catalysis,[19,28–30] separation techniques,[31] polymers[32,33] and medicinal chemistry.[34,35] The C–F bond of fluorocarbons is stronger as well as longer compared to the C–H bond. The electronegativity of fluorine is higher which makes the C–F group less polarizable as compared to the C–H group. In addition, the dipole moment of the C–F bond is higher and the direction is opposite to the C–H bond.[36] These properties combinedly make the C–F group containing molecules inert, extremely hydrophobic and less polarizable, which endows them with unusual phase segregation properties *via* weak F···F fluorous interactions.

Fluorinated ETHs are important molecules which show unique physicochemical properties due to the presence of the C–F group. Fluorinated alcohols generally have higher melting as well as lower boiling points than their non-fluorinated counterparts which makes them useful in polymers[32,33] as well as medicinal chemistry.[34,35] Moreover, fluorinated alcohols stabilize the secondary structure of proteins.[37–39] In order to understand the unique behavior of fluorinated alcohols, several groups have explored their hydrogen bond network in bulk[15] as well as in the gas phase.[16,17,40–42] A supersonic jet study of dimers and trimers of fluorinated-ETHs clearly shows that apart from the O–H···O hydrogen bond, O–H···F interactions play a significant role in their stabilization.[43] We have also studied monofluoroethanol (MFE) in bulk medium and found the existence of a significant

Department of Spectroscopy, Indian Association for the Cultivation of Science, Kolkata, India. E-mail: sppcs@iacs.res.in

† Electronic supplementary information (ESI) available: The detailed description of the deconvolution of the OH band, NMR and IR data for the C–F group of MFE in an aqueous mixture. See DOI: 10.1039/c7cp04663d

amount of O–H···F interactions in bulk medium.[15] Recently, Shum and coworkers concluded that a single C–F substitution on ETH changes the role of the first water molecule from a donor to an acceptor as compared to ETH under isolated gas phase conditions.[18] However, the hydrogen bond network in bulk medium is more complicated than that in the gas phase as the hydrogen bonds between different species of mixtures will compete with each other throughout different compositions of water in alcohol mixtures. Hence, it will be interesting to explore the effect of single fluorine substitution on the hydrogen bond network of an aqueous mixture of ETH.

In this paper, we have investigated the hydrogen bond network of aqueous mixtures of ETH and MFE using the deconvolution of IR bands in the OH stretching region, molecular dynamics (MD) simulations and quantum chemical calculations coupled with AIM analysis to understand the role of water molecules as well as the C–F group of MFE in the hydrogen bond network. Infrared spectroscopy of the donor stretching frequency is very sensitive to the hydrogen bonding environment, and hence, the OH stretching region has been probed for different mole fractions of water in their alcohol mixtures. MD simulations as well as quantum chemical calculations and AIM analysis have been used to decipher the experimental data in order to understand the role of alcohols (MFE and ETH) and water as a donor or acceptor along with the nature of their interactions in the respective hydrogen bond networks. This study clearly reveals that fluorination of ETH changes the hydrogen bonding site of water from the oxygen terminal of the alcohol to a fluorine site which decreases the clustering of water and simultaneously, increases the hydrogen bonding between the alcohol and water molecules.

Methods

The infrared spectra of the mixtures in the range of 3000–3800 cm^{-1} have been measured by a Fourier transformed infrared spectrometer (Nicolet iS10, Thermo Fisher) operating in the attenuated total reflection (ATR) mode and equipped with a DTGS detector. The ATR crystal (PIKE, Gladi-ATR) is made of a monolithic diamond crystal with an incident angle of 45°. The resolution of the IR measurements was 2 cm^{-1}. Extended ATR correction has been performed for the measured IR spectra. A flow of N_2 gas was used throughout the measurements to remove the effect of atmospheric vapors. All measurements have been performed at room temperature (25 ± 3 °C). The data acquisition has been performed by the OMINI software. ETH (99.9%) and MFE (98%) were purchased from Spectrochem (Mumbai, India) and dried using molecular sieves prior to all measurements. We have also measured the IR spectra of pure alcohols in the water bending region in order to make sure that the pure alcohol solutions are not contaminated by water. Purified water (H_2O, Millipore, resistivity: 18.2 MΩ cm) was used to make the aqueous mixtures of ETH and MFE.

MD simulations of the aqueous mixtures of ETH and MFE were carried out using the all atom simulation method incorporated in the GROMACS molecular dynamics simulation package.[44] The all atom (OPLS-AA) parameters for ETH and the TIP5PE parameters for water were used as available in GROMACS topology, whereas, the topology of MFE was constructed using automated topology builder (ATB) software[45,46] by attaining the correct density of MFE *via* tuning of its partial charges. Each simulation box contains ~4000 alcohol and water molecules. For each case, we have run 1000 steps of steepest descent followed by 10 000 steps of a conjugate gradient energy minimization algorithm to exclude all unfavorable interactions from the initial configuration. Each trajectory was further equilibrated in an *NVT* ensemble at 800 K for 500 ps to remove the biased dependencies on the initial configuration followed by an equilibration in the *NPT* ensemble at 300 K and 1 bar pressure for 1 ns. Subsequently, the equilibrated configuration was subjected to a production run of another 5 ns in the *NPT* ensemble at 300 K and 1 bar pressure. The temperature as well as pressure of the system were kept constant using the Berendsen thermostat[47] with a time constant (τ) of 0.1 ps^{-1} and the Parinello–Rahman barostat[48] with a τ of 1.0 ps^{-1}, respectively. Electrostatic interactions were incorporated by particle Mesh Ewald (PME) calculations.[49] Each simulation used a time step of 2 fs with the periodic boundary conditions. Neighbor list generation has been performed with the help of non-bonded force calculations with a grid and updated after 5 steps throughout the simulation. A cut-off radius of 1.2 nm was used both for the neighbor list and van der Waals interaction. We have calculated the coordination number using the default option in GROMACS.

The different types of 1:1 clusters of ETH–water and MFE–water complexes have been optimized in their bulk media using the B3LYP method with the 6-311++G(d,p) basis set. The solvent effect has been incorporated using the polarizable continuum model (PCM). Frequency calculations have been performed for all the structures in their bulk media in order to confirm the nature of the optimized structures. The frequencies were found to be real for all the structures assuring that the particular structure is a minimum energy structure. We have also performed the anharmonic frequency calculations for all the structures. Optimization has been performed with standard convergence criteria and frozen core approximation. The population of each cluster has been calculated using the Gibbs free energies of the respective cluster. The stabilization energy has been calculated using the supramolecular approach and further corrected for the basis set superposition error. All the calculations have been performed using the G09 suite of program.[50] Furthermore, AIM calculations have been performed to characterize the nature of interaction between different groups of clusters.[51]

Results and discussion

(a) Experimental IR study

The OH stretching frequency of water and alcohol is extremely sensitive to the local hydrogen bond environment. In order to understand the hydrogen bond network of the aqueous mixtures of ETH and MFE, we have measured the IR spectra of mixtures

in their OH stretching region. Fig. 1a shows the IR spectra of the ETH–water mixture in the OH stretching region (3050–3750 cm^{-1}) with an increasing mole fraction of water in the mixture. The IR spectrum of pure water (red line, Fig. 1a and b) is broad covering the OH stretching region of 3050–3800 cm^{-1} with a double peak feature centered around 3250 cm^{-1} and 3370 cm^{-1}. Some authors have assigned the peak at ~3200 cm^{-1} to water molecules organized in an ordered tetrahedral symmetric long range hydrogen bond network, whereas, the peak at ~3370 cm^{-1} has been assigned to an asymmetric tetrahedral hydrogen bonded network.[52] In contrast, some authors have assigned the double peak feature around 3200 and 3370 cm^{-1} to the Fermi resonance between the OH stretching and two quanta of the bending modes.[52,53] The IR spectrum of pure ETH shows a broad single peak centered around 3330 cm^{-1} (Fig. 1a, gold line) which indicates the absence of intramolecular coupling in bulk ETH. The IR spectrum of MFE is much broader as well as blue shifted compared to ETH, centered around 3350 cm^{-1} with an additional broad feature in the high frequency region around 3550–3660 cm^{-1} peaked at ~3580 cm^{-1} (Fig. 1b, gold line). The broad feature of MFE as compared to ETH shows the presence of different types of hydrogen bond in MFE than ETH. A blue shift in the IR spectrum of MFE shows that the average hydrogen bond strength of MFE is weaker as compared to ETH. In our earlier study, we have assigned the broad peak in the region of 3000–3550 cm^{-1} to the different sizes of O–H···O hydrogen bonded clusters, whereas, the peak at the high frequency region ~3580 cm^{-1} has been assigned to the intermolecular O–H···F interaction present in bulk MFE.[15] Indeed, in the earlier supersonic jet study for the MFE dimer, a vibrational band at ~3590 cm^{-1} has been found which was assigned to the O–H···F interaction between MFE dimers.[53]

In order to simplify the discussion about the change in the spectral shape of the aqueous mixtures of ETH and MFE, we have divided them into three regions, (a) water rich region ($0.97 \geq X_w \geq 0.80$), (b) intermediate region ($0.79 \geq X_w \geq 0.25$), and (c) alcohol rich region ($X_w \leq 0.25$). The spectral shape of the aqueous mixture of ETH is significantly different from that of MFE in the water rich region as shown in Fig. 1c. The addition of a small amount of ETH in pure water increases the intensity ratio of IR peaks at 3200 cm^{-1} and 3370 cm^{-1} compared to the case of pure bulk water and this trend is clearly visible between $0.97 \geq X_w \geq 0.83$ compositions (Fig. 1c, first plot). The shape of IR spectra in the OH stretching region is governed by the hydrogen bonds between water and alcohol as well as water–alcohol molecules which compete with each other at different compositions. However, the hydrogen bond between water molecules as well as water–alcohol hydrogen

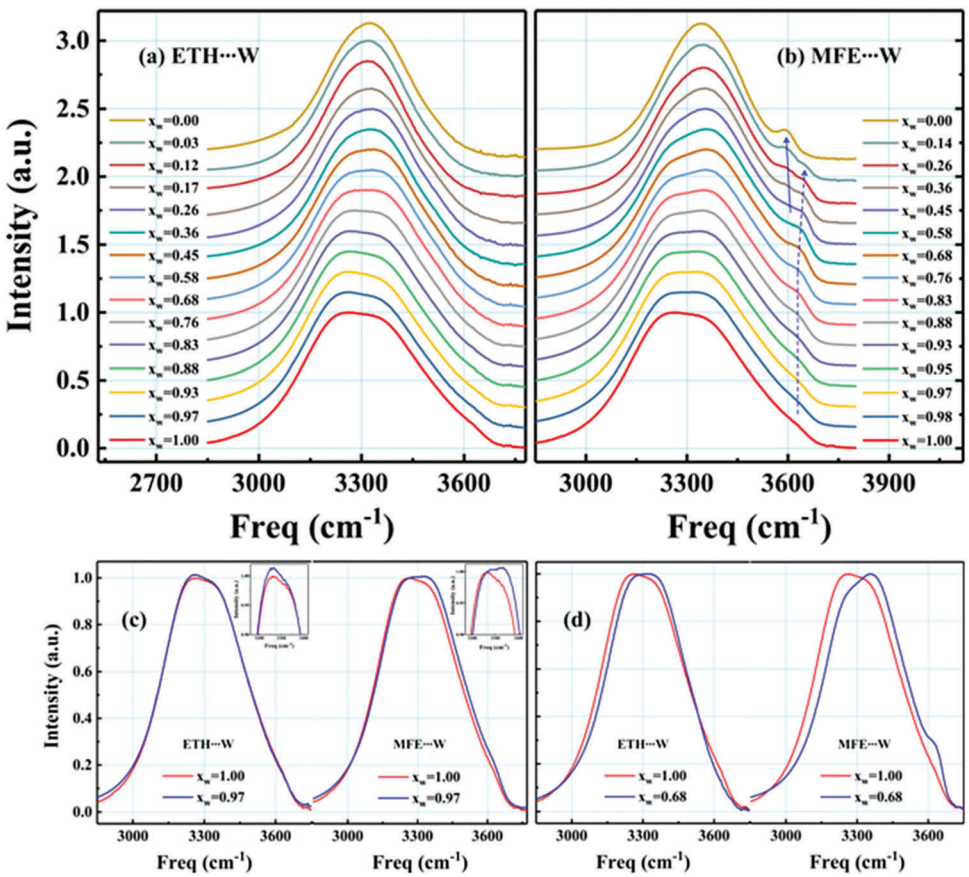

Fig. 1 IR spectra in the OH stretching region of ETH–water (a) and MFE–water (b) mixtures. The offset in the figures has been provided for clarity. (c and d) A comparison of the intensity of the bands at 3200 and 3370 cm^{-1} for the ETH–water and MFE–water mixtures at X_w = 0.97 and 0.68 with pure bulk water (X_w = 1.00). The figures in the inset of (c and d) are shown for clarity of the visualization of the band intensity.

bonds will compete with each other in the water rich region of the aqueous mixture of the alcohol due to the lower concentration of alcohol in the mixture. The increased intensity of the IR peak at 3200 cm^{-1} in the water reach region of ETH ($0.97 \geq X_w \geq 0.83$) has been mainly assigned to the increased clusterization of water through strong O–$H_w\cdots O_w$ hydrogen bonds as the water–alcohol hydrogen bonds appear at $\sim$3400 cm^{-1}. In contrast to ETH, the intensity ratio of IR peaks at 3200 cm^{-1} and 3370 cm^{-1} decreases as compared to pure bulk water on addition of a small amount of MFE in pure water ($X_w = 0.97$) (Fig. 1c, second plot). The increased intensity of the peak $\sim$3370 cm^{-1} with the addition of MFE in an aqueous medium suggests that the contribution of hydrogen bonds between water and MFE is more prominent than the O–$H_w\cdots O_w$ hydrogen bonds between water molecules. Noticeably, a new band at the high frequency region of the OH stretching frequency at $\sim$3640 cm^{-1} appears simultaneously (Fig. 1c) on addition of MFE ($X_w \leq 0.98$) in an aqueous medium and its intensity keeps on increasing with the further addition of MFE (blue dotted line, Fig. 1b) suggesting the presence of an extremely weak interaction between water and MFE. We tentatively assigned the peak at $\sim$3640 cm^{-1} to the O–$H_w\cdots F_{MFE}$ interaction between the OH group of water and the fluorine of MFE. Indeed, water at the air/water as well as lipid interfaces shows a peak at around $\sim$3650 cm^{-1} which has been assigned to the water in the hydrophobic environment.[54,55] The IR data for the aqueous mixture of MFE in the water rich region indicates that the population of strong O–$H_w\cdots O_w$ hydrogen bonded water species decreases at the cost of the increased population of weakly interacting O–$H_w\cdots F_{MFE}$ species.

In the intermediate region of the aqueous mixture of ETH as well as MFE, the intensity of the 3370 cm^{-1} peak is higher than that at 3200 cm^{-1} and the center peak position is blue shifted compared to pure water (Fig. 1d). The amount of increase in the intensity of the peak at 3370 cm^{-1} as well as the blue shift of the center of the peak position is higher for the aqueous mixture of MFE than ETH (Fig. 1d). The blue shift in the centre of the peak position with the addition of alcohol indicates the weakening of the average hydrogen bonds of the mixture compared to pure water indicating the increase of the hydrogen bonds between the alcohol and water at the cost of the O–$H_w\cdots O_w$ hydrogen bonds between the water molecules which simultaneously enhances the intensity of the peak at $\sim$3370 cm^{-1} as the hydrogen bond between the water and alcohol appears at $\sim$3400 cm^{-1}. For the aqueous mixture of MFE, the peak appearing in the high frequency region at $\sim$3640 cm^{-1} becomes more intense with further addition of MFE in the intermediate region indicating the further increase of the population of weakly interacting O–$H_w\cdots F_{MFE}$ species. The increased intensity of the appearance of the high frequency peak in the case of MFE in the intermediate region suggests that water interacts with fluorine as well as oxygen terminals of MFE whereas the interaction of water is taking place only towards the oxygen terminal of ETH.

In the alcohol rich region, the IR spectra of the aqueous mixture of ETH converge to one peak centered at $\sim$3330 cm^{-1} indicating that the hydrogen bond environment of the aqueous mixture of ETH is similar to pure ETH and dominated by ETH clusters. In the case of the MFE–water mixture, one peak centered at around 3350 cm^{-1} appears and the intensity of the IR peak in the high frequency region at 3640 cm^{-1} decreases with the emergence of a new peak at $\sim$3600 cm^{-1} whose intensity increases afterwards. The appearance of a single peak with further addition of MFE in the aqueous mixture indicates that the environment of the mixture ($X_w < 0.68$) is more like pure bulk MFE. Moreover, the simultaneous appearance of a new peak at $\sim$3600 cm^{-1} and the disappearance of the peak at 3640 cm^{-1} indicates that the O–$H_w\cdots F_{MFE}$ interaction between the water and MFE decreases and O–$H_{MFE}\cdots F_{MFE}$ interaction between MFE increases.

Furthermore, to quantify the contribution of the different hydrogen bonded species in the aqueous mixture of alcohol, we have deconvoluted the IR spectra in the O–H stretching region using the method proposed by Walrafen as well as Gadomski *et al.* (Fig. S1, ESI†).[52,56] The OH band of the ETH–water mixtures has been deconvoluted using seven Gaussian peaks. Five Gaussian peaks centered at 3080, 3200, 3400, 3500, and 3600 cm^{-1} belong to the water-like part[57,58] and two of them at around 3280, and 3360 cm^{-1} correspond to the ETH clusters.[59] The peak at 3080 cm^{-1} has been assigned to the Fermi resonance between the overtone of the bending mode (1630 cm^{-1}) and the 3200 cm^{-1} stretching mode of the water molecule. The peak at around 3200 cm^{-1} belongs to the water molecules organized in the symmetrical tetrahedral ordered long-range hydrogen bonding network whereas the peak at 3400 cm^{-1} has been assigned to either the not in-phase vibrations between the higher-neighbor water molecules or the asymmetric tetrahedral hydrogen bonded network.[57,60] The peaks at in the high frequency region at around 3500 and 3600 cm^{-1} [52,57,58] have been assigned to the weakly hydrogen bonded water molecules. The experimental IR spectra and the results of deconvolution for the different mole fraction of water in the ETH–water mixture are shown in Fig. S2 (ESI†). All the peaks are normalized with respect to the total area which is the sum of the areas of five water peaks and two alcohol peaks and the relative areas are shown in Table 1. In the water rich region of the aqueous mixture of ETH, it can be seen that the contribution of the peak at 3200 cm^{-1} increases and simultaneously the contribution of the peak in the high frequency regions ($\sim$3500 cm^{-1}) as well as the contribution of the peak at 3400 cm^{-1} decreases (Fig. S3, ESI†). On the basis of fitting, we conclude that the addition of a small amount of water in ETH increases the contribution of water molecules arranged in a tetrahedral hydrogen bonded network (3200 cm^{-1}) as compared to the bulk water at the cost of the weakly hydrogen bonded water molecules (3500 and 3600 cm^{-1}). This result is in good agreement with the earlier prediction that the self-aggregation of water increases in the second hydration shell of ETH in the water rich region of the aqueous mixture.[61] In the intermediate region of the aqueous mixture, the contribution of the ETH component (mainly in the region of 3400 cm^{-1}) increases (Fig. S3, ESI†). The increase of the ETH peak at 3400 cm^{-1} may be because of ETH clustering as well as the water–ETH hydrogen bonding. However, in the intermediate region of the mixture, the contribution from the hydrogen

Table 1 The deconvoluted contribution of the different peaks for water and alcohol in different compositions of the aqueous mixture of ETH and MFE

	Water					
X_w	3050	3200	3400	3500	3600	ETH
(a) ETH–water mixture						
1.00	0.091	0.454	0.310	0.101	0.044	
0.97	0.082	0.460	0.308	0.062	0.037	0.056
0.93	0.069	0.461	0.307	0.063	0.030	0.073
0.88	0.068	0.465	0.303	0.060	0.032	0.077
0.83	0.060	0.450	0.290	0.087	0.035	0.082
0.76	0.071	0.399	0.269	0.082	0.046	0.132
0.68	0.057	0.361	0.234	0.115	0.043	0.190
0.58	0.062	0.315	0.200	0.136	0.040	0.247
0.45	0.078	0.260	0.155	0.136	0.037	0.334
0.36	0.070	0.230	0.140	0.125	0.039	0.396
0.27	0.084	0.222	0.142	0.123	0.024	0.406
0.17	0.072	0.157	0.096	0.112	0.019	0.545
0.12	0.069	0.072	0.047	0.072	0.008	0.733
0.03	0.054	0.027	0.034	0.033	0.010	0.842
0.00						1.000

	Water						Water–MFE
X_w	3050	3200	3400	3500	3600	MFE	3640
(b) MFE–water mixture							
1.00	0.091	0.454	0.310	0.101	0.044		
0.98	0.074	0.357	0.315	0.104	0.041	0.100	0.012
0.97	0.074	0.322	0.324	0.100	0.042	0.126	0.012
0.95	0.074	0.313	0.317	0.099	0.039	0.147	0.011
0.93	0.075	0.276	0.321	0.102	0.040	0.174	0.014
0.88	0.065	0.274	0.295	0.100	0.030	0.218	0.017
0.83	0.062	0.265	0.267	0.117	0.032	0.243	0.015
0.76	0.054	0.242	0.178	0.182	0.020	0.308	0.017
0.68	0.048	0.216	0.131	0.202	0.020	0.364	0.019
0.58	0.037	0.181	0.093	0.195	0.028	0.449	0.017
0.45	0.035	0.133	0.084	0.182	0.035	0.520	0.011
0.36	0.025	0.113	0.068	0.113	0.056	0.618	0.008
0.26	0.019	0.076	0.050	0.076	0.050	0.722	0.007
0.14	0.015	0.030	0.025	0.024	0.036	0.864	0.006
0.00					0.029	0.971	

bonding between ETH–water will dominate over the clustering of ETH molecules. Simultaneously, in the intermediate region of the aqueous mixture of ETH, the contribution of the water peak at 3200 cm^{-1} decreases and the contribution of the weak hydrogen bonded water molecules ($\sim$3500 cm^{-1}) increases slightly. The spectral change of the aqueous mixture of the ETH–water mixture in the intermediate region indicates that a tetrahedral hydrogen bonded structure of water is broken or loosened and the loosened water cluster interacts strongly with the ETH molecules. Indeed, the quick increase of the excess compressibility of the aqueous mixture of ETH has been observed in the intermediate region which has been assigned to the decrease of the tetrahedral hydrogen bonded structure of water in this region.[62]

In contrast to ETH, for the deconvolution of the spectra of an aqueous mixture of MFE, we have to use an additional peak at 3640 cm^{-1} which originates due to the $O–H_w\cdots F_{MFE}$ hydrogen bond as discussed earlier. In the water rich region, unlike the ETH–water mixture, the contribution of the water peak at the 3200 cm^{-1} decreases and the peak at the 3400 cm^{-1} increases (Fig. S3, ESI†). In addition, the contribution of the peak at $\sim$3640 cm^{-1} increases and the contribution of MFE increases, and this increase is more than that in the case of ETH. The spectral shape of the aqueous mixture of MFE in a water rich region suggests that the tetrahedral hydrogen bonded structure is broken or loosened. Water is in an asymmetrical hydrogen bonding environment due to the hydrogen bonding with MFE *via* $O–H_{w/MFE}\cdots O_{MFE/w}$ and $O–H_w\cdots F_{MFE}$ interactions. In the intermediate region, the contribution of the MFE part as well as the population of the peak at 3640 cm^{-1} increases further indicating the increased contribution of $O–H_{w/MFE}\cdots O_{MFE/w}$ and $O–H_w\cdots F_{MFE}$ interactions. Simultaneously, the contribution of the water peak at 3200 cm^{-1} decreases further and the contribution of the peak at 3500 cm^{-1} increases. The spectral change of the aqueous mixture in the MFE–water mixture in the intermediate region indicates that the tetrahedral hydrogen bonded structure of water is broken or loosened and the loosened water cluster interacts strongly with the MFE molecules. In the alcohol reach region, apart from the increase in the contribution of MFE, the contribution of the peak at 3600 cm^{-1} increases which is due to the increased clusterization of MFE through $O–H_{MFE}\cdots F_{MFE}$ interaction. The quantitative and qualitative analysis of the IR spectra of the different compositions of the aqueous mixture of ETH and MFE clearly shows that the C–F group of MFE affects its interaction with water molecules which creates the difference between the hydrogen bond network of aqueous mixtures of ETH and MFE.

(b) Molecular dynamics simulation

To understand the role of the C–F group of MFE on the impact of the water organization around the MFE, we have calculated $g(r)$ at different binding sites of alcohol and water in their respective aqueous mixtures. Fig. 2 shows the $g(r)$ between hydrogen and oxygen of alcohols as well as water for different compositions of alcohol–water mixtures. The intensity of the first peak of $g(r)$ between hydrogen and oxygen of ETH decreases with the increase of water (Fig. 2a), whereas, the intensity of the first peak of $g(r)$ between hydrogen and oxygen of water increases with the increase of ETH (Fig. 2b), in their aqueous mixture. The $g(r)$ plots for oxygen and water indicate that the addition of water decreases the association of ETH molecules *via* $O–H_{ETH}\cdots O_{ETH}$ hydrogen bonds, however, the association of water through $O–H_w\cdots O_w$ hydrogen bonds increases with the increase of ETH in their aqueous mixtures. It can be inferred that ETH is a less associating and water is a more associating species in the aqueous mixture of ETH.

Similar to the case of the ETH–water mixture, the intensity of the first peak of $g(r)$ between hydrogen and oxygen of MFE decreases on the addition of water (Fig. 2c). However, the extent of the decrease of $g(r)$ is higher in the case of MFE–water mixtures as compared to ETH–water which indicates that the association of MFE through $O–H_{MFE}\cdots O_{MFE}$ hydrogen bonds decreases rapidly as compared to ETH in their aqueous mixtures. Unlike the ETH–water mixture, the intensity of the first peak of $g(r)$ between the hydrogen and oxygen of water (Fig. 2d) increases up to $X_w = 0.7$ and after that it decreases with the increase of MFE in their aqueous mixture indicating that

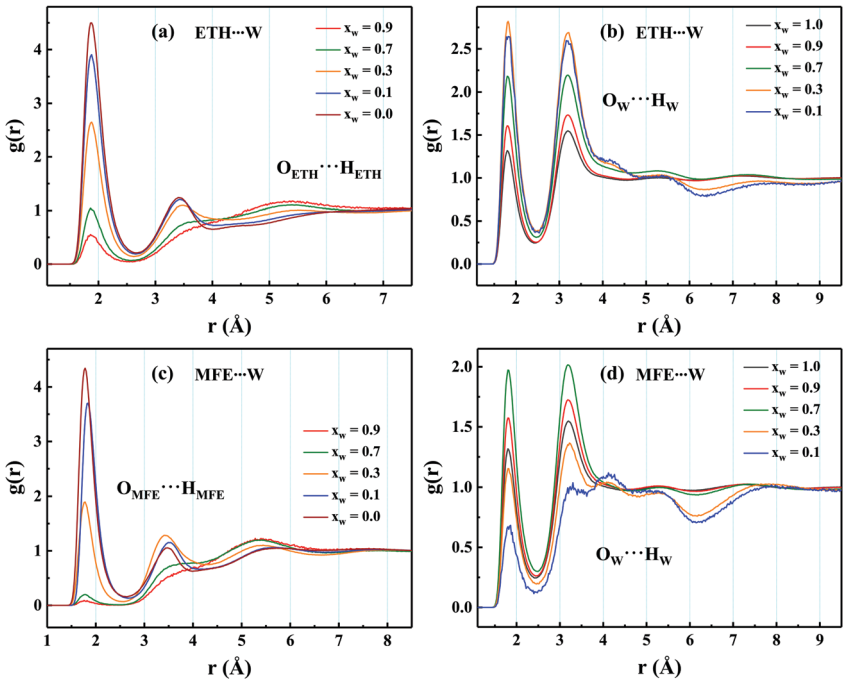

Fig. 2 The $g(r)$ between oxygen and hydrogen of the OH group of ETH (a) and water (b), respectively in the aqueous mixture of ETH and the $g(r)$ between oxygen and hydrogen of the OH group of MFE (c), and water (d), respectively in the aqueous mixture of MFE.

the association of water through the O–$H_w\cdots O_w$ hydrogen bond gets perturbed *via* another interaction of water molecules after $X_w = 0.7$. It is also noticeable that the increase in the intensity of the $g(r)$ of water up to $X_w = 0.7$ of MFE–water is less as compared to the case of ETH–water suggesting that the association of water through O–$H_w\cdots O_w$ hydrogens bond is less in the aqueous mixtures of MFE as compared to the ETH–water mixture. The different trend of self association of water and alcohol for the aqueous mixture of MFE and ETH strongly suggests that fluorine of MFE plays a significant role in the hydrogen bond network of the aqueous mixture of MFE.

In order to understand the role of fluorine in the hydrogen bond network of the aqueous mixture of MFE, we have calculated $g(r)$ between the hydrogen of the OH and fluorine of MFE as well as the hydrogen of the OH of water and fluorine of MFE as shown in Fig. 3. The first peak position of the $g(r)$ between hydrogen of the OH and fluorine of MFE (Fig. 3a) gets shifted towards higher distance and the intensity of the peak increases with the increase of the water content in the aqueous mixture of MFE. The $g(r)$ between hydrogen of OH and fluorine of MFE suggests that MFE associates mainly *via* the O–$H_{MFE}\cdots F_{MFE}$ interaction with the increase of the water content which is also justified by the less association of MFE *via* O–$H_{alc}\cdots O_{alc}$ hydrogen bonds as compared to ETH in their respective aqueous mixtures. The intensity of the first peak of $g(r)$ between the hydrogen of water and fluorine of MFE increases with the increase of MFE which is significant after $X_w \sim 0.7$ of the aqueous mixture of MFE (Fig. 3b). The intensity of the first peak of $g(r)$ between the hydrogen of water and fluorine of MFE indicates that the O–$H_w\cdots F_{MFE}$ interaction between the water and MFE is less until $X_w \geq 0.7$ and becomes prominent after $X_w \leq 0.7$. This observation is in good agreement with the

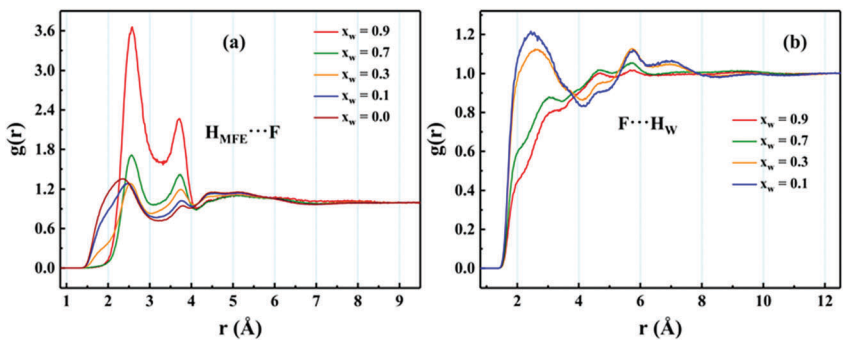

Fig. 3 The $g(r)$ between (a) the hydrogen of OH and fluorine of MFE and (b) the hydrogen of the OH group of water and fluorine of MFE for different compositions of MFE–water mixtures.

experimental IR data as the intensity of the high frequency peak at $\sim$3600 cm^{-1} which has been assigned to O–H$_w\cdots$F$_{MFE}$ interaction keeps on increasing with the increase of MFE until $X_w \sim 0.7$. The O–H$_w\cdots$F$_{MFE}$ interactions in the aqueous mixture of MFE take place at the cost of the O–H$_w\cdots$O$_w$ hydrogen bond between the water molecules, hence, the clusterization of water decreases after $X_w < 0.7$. In summary, the $g(r)$ data between the OH sites of alcohols and water along with the fluorine site of MFE in their aqueous mixtures reveals that the association of alcohols through the O–H$_{alc}\cdots$O$_{alc}$ hydrogen bond decreases upon addition of water. The association of water through O–H$_w\cdots$O$_w$ increases with the increase of ETH in their aqueous mixture, however, the association of water through O–H$_w\cdots$O$_w$ decreases after a certain composition in the aqueous mixture of MFE due to the significant increase of O–H$_w\cdots$F$_{MFE}$ interaction. It is distinctly clear from the simulation that the presence of the fluorine reorganizes the hydrogen bonding in the aqueous mixture of MFE by compelling water to act more as a hydrogen bond donor *via* the O–H$_w\cdots$F$_{MFE}$ interaction and simultaneously decreases the water clustering *via* O–H$_w\cdots$O$_w$ hydrogen bonds. This result is in good agreement with the experimental IR results where the clustering of water increases with the addition of ETH whereas it decreases in the case of the aqueous mixture of MFE in their water rich region.

Furthermore, we have investigated the intermolecular hydrogen bonding between water and alcohols in the hydrogen bond network of their aqueous mixtures by calculating the $g(r)$ between hydrogen of the OH of alcohols and oxygen of water and *vice versa* as shown in Fig. 4. The intensity of the first peak of $g(r)$ plots between hydrogen of the OH of ETH and oxygen of water and *vice versa* (Fig. 4a and b) for the aqueous mixture of ETH shows that the number of O–H$_{ETH}\cdots$O$_w$ hydrogen bonds is higher compared to the O–H$_w\cdots$O$_{ETH}$ hydrogen bonds. The $g(r)$ plots between the water and ETH depict that the hydrogen bond donating capability of ETH is higher compared to water in the hydrogen bond network of the aqueous mixture of ETH. The intensity of the first peak of $g(r)$ plots between the hydrogen of the OH of MFE and oxygen of water and *vice versa* for the aqueous mixture of MFE (Fig. 4c and d) follows a similar trend to an aqueous mixture of MFE suggesting that the number of O–H$_{MFE}\cdots$O$_w$ hydrogen bonds is higher compared to the O–H$_w\cdots$O$_{MFE}$ hydrogen bonds in their aqueous mixture. However, for the aqueous mixture of MFE, the intensity of the first peak of $g(r)$ between the hydrogen of OH of alcohol and oxygen of water is approximately two times higher and simultaneously, the intensity of the first peak of $g(r)$ between the hydrogen of OH of water and oxygen of alcohol is $\sim$1.5 time lower as compared to the aqueous mixture of ETH, which reflects that the OH of MFE is a comparatively strong hydrogen bond donor to water compared to ETH in their aqueous mixture.

We have also calculated the CN for the different interactions in the aqueous mixtures of alcohol and the results are shown in Fig. 5. It can be seen that the CN for the self-association of alcohol and water is more in the case of ETH than MFE in their aqueous mixture. The CN for the interaction of fluorine with the hydrogen of OH of MFE decreases with the increase of water content and simultaneously, the significant increase in the CN for the interaction of fluorine with hydrogen of water clearly manifests that the O–H$_w\cdots$F$_{MFE}$ interaction is significant.

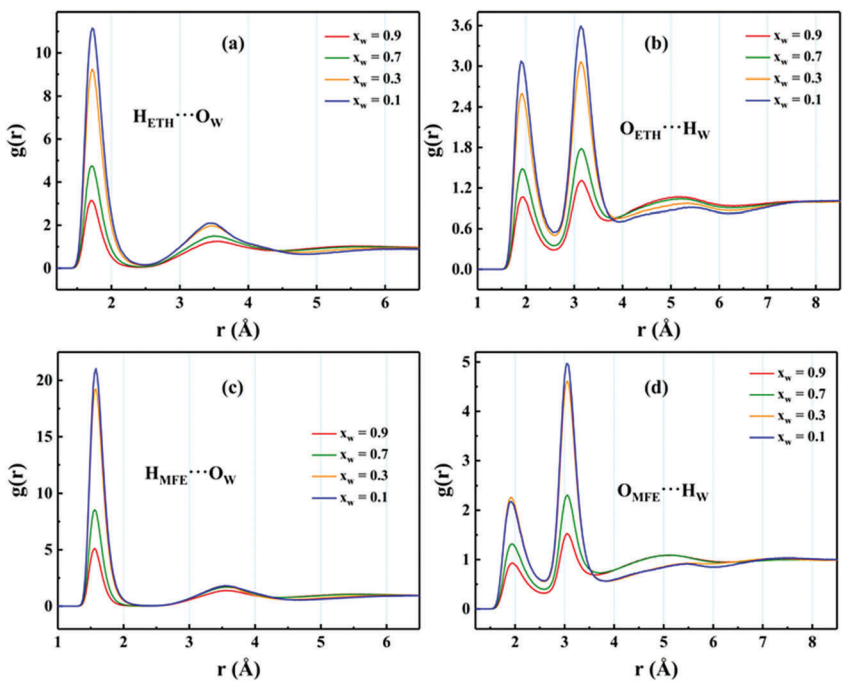

Fig. 4 The $g(r)$ plots between the hydrogen of the OH group of ETH and oxygen of water molecules (a), and the hydrogen of the OH group of water and oxygen of OH of ETH molecules in the ETH–water mixtures (b). Similarly, the $g(r)$ plots between the hydrogen of the OH group of MFE and oxygen of water molecules (c) and the hydrogen of the OH group of water and oxygen of OH of MFE molecules (d) in the MFE–water mixtures.

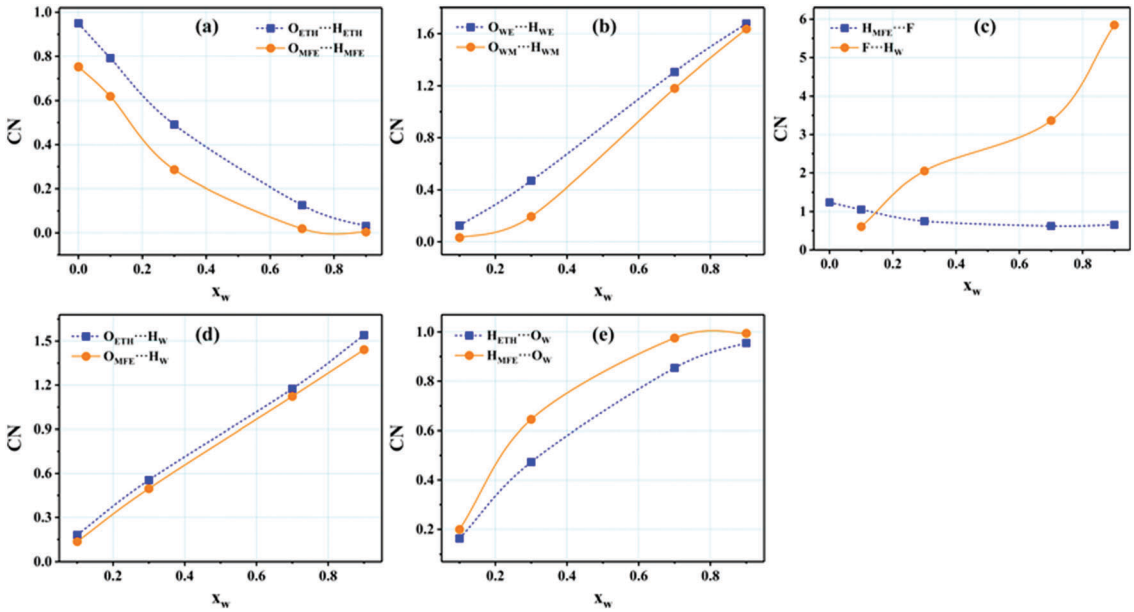

Fig. 5 The coordination number for the different interactions of the aqueous mixture of ETH and MFE.

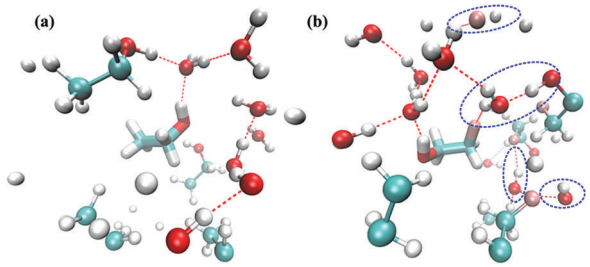

Fig. 6 Snapshots of the aqueous mixture of ETH (a) and MFE (b) for X_w = 0.7. The blue line in the aqueous mixture of MFE shows the $O–H_w\cdots F_{MFE}$ interactions which induce the $O–H_{MFE}\cdots O_w$ hydrogen bonds.

The CN for the $O–H_w\cdots O_{alc}$ interaction is slightly higher for the case of ETH than MFE, however, the CN for the $O–H_{alc}\cdots O_w$ is significantly high for the MFE than ETH in their aqueous mixture clearly suggesting that the OH of MFE is a strong hydrogen bond donor to water as compared to ETH. The increased donating capability of the OH group of MFE to the water molecule is due to the increased $O–H_w\cdots F_{MFE}$ interaction in the aqueous mixture of MFE which is in good agreement with the radial distribution calculations.

The CN, $g(r)$ calculations along with the experimental IR data suggest that the fluorination of ETH causes switching of the orientation as well as hydrogen bonding sites of water molecules in which the OH of water interacts mainly with the fluorine of MFE *via* $O–H_w\cdots F_{MFE}$ interactions. Due to the $O–H_w\cdots F_{MFE}$ interactions, oxygen of water is more accessible for the $O–H_{MFE}\cdots O_w$ hydrogen bond *via* the cyclic structure (as shown in Fig. 6) which makes the MFE a stronger hydrogen bond donor as compared to the ETH in their aqueous mixture. Moreover, due to the $O–H_w\cdots F_{MFE}$ interaction, the clustering of water *via* $O–H_w\cdots O_w$ interactions decreases compared to the case of ETH in their aqueous mixture.

(c) Quantum chemical study

MD simulation only provides information about the solvent organization and the probable interactions. Hence, to confirm the correlation of experimental IR data with MD simulation as well as to describe the nature of different interactions involved between water and alcohol, we have performed quantum chemical calculations on the 1 : 1 cluster of ETH–water and MFE–water in an aqueous medium using the B3LYP/6-311++G(d,p) level of theory. Furthermore, AIM analysis has been performed to get insight into the nature of different interactions of all the structures. Fig. 7 describes the optimized structures of ETH–water and MFE–water clusters in an aqueous medium along with the critical points between the different interactions. The stabilization energy and vibrational frequency as well as the topological

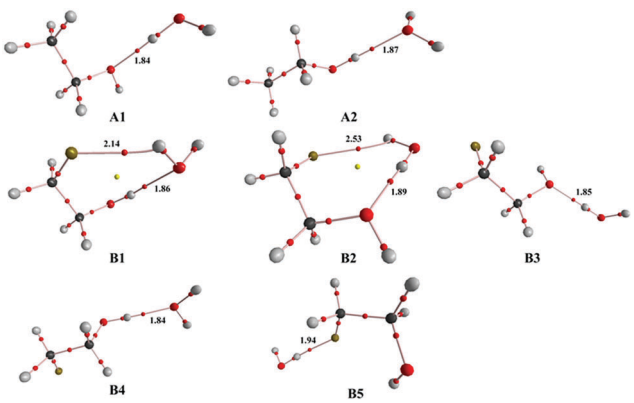

Fig. 7 The optimized structures of 1 : 1 clusters of ETH–water (A1 and A2) and MFE–water (B1 to B5) using the B3LYP/6-311++G(d,p) level of theory using the PCM model to incorporate the solvent effect. The (3, −1) and (3, +1) critical points for each structure have been shown in the red and yellow balls respectively.

Table 2 The stabilization energy (ΔE, kcal mol^{-1}), change in vibrational frequency ($\Delta\nu$, cm^{-1}), electron density ($\rho_{(c)}$), and Laplacian (∇^2) for the 1:1 clusters of ETH–water and MFE–water calculated at the B3LYP/6-311++G(d,p) level of theory

	ΔE	$\Delta\nu_{(H_2O)}$	$\Delta\nu_{(OH\ alc)}$	$\Delta\nu_{(CF\ MFE)}$	$\rho_{(c)}$	∇^2
ETH–W						
A1	4.4	3627 (−91), 3573 (−80)	3457 (−193)		0.0306	0.111
A2	4.0	3634 (−84), 3391 (−263)	3637 (+15)		0.0282	0.106
MFE–W						
B1	4.6	3701 (−17), 3630 (−20)	3400 (−223)	973 (−7)	0.031, 0.014	0.055, 0.105
B2	4.3	3451 (−182), 3691 (−17)	3649 (+26)	978 (−2)	0.027, 0.007	0.028, 0.103
B3	4.2	3435 (−198), 3692 (−16)	3640 (+17)	983 (+3)	0.029	0.103
B4	4.0	3714 (−4), 3629 (−4)	3593 (−206)	1004 (+25)	0.030	0.104
B5	2.1	3699 (−19), 3615 (−38)	3634 (+11)	960 (−20)	0.020	0.084

$\Delta\nu_{(H_2O)}$ represents the change in the OH stretching of water, $\Delta\nu_{(OH\ alc)}$ represents the change in the OH stretching of alcohol, and $\Delta\nu_{(CF\ MFE)}$ represents the change in the C–F stretching frequency.

parameters such as electron density (ρ) and the Laplacian (∇^2) at the BCPs are depicted in Table 2. ETH–water clusters form both O–H$_w\cdots$O$_{ETH}$ (A1) and O–H$_{ETH}\cdots$O$_w$ (A2) hydrogen bonded complexes out of which the stabilization energy as well as the relative population (60%) of structure A1 is slightly higher than A2 (40%). The presence of (3, −1) BCP with a positive ∇^2 value for both O–H$_w\cdots$O$_{ETH}$ and O–H$_{ETH}\cdots$O$_w$ interaction shows the presence of non-covalent interactions. The vibrational frequency data for the ETH–water cluster shows that the OH of water interacting with alcohol (structure A1) appears at around $\sim$3400 cm^{-1} whereas the alcohol OH interacting with the water (structure A2) appears at $\sim$3450 cm^{-1}. Vibrational frequency calculations of the ETH–water cluster assure that the observed increased intensity of the IR peak at $\sim$3200 cm^{-1} in the water rich region is due to the water clustering and it has no contribution from the water–ETH hydrogen bond. Further, it also shows that the increased intensity of the peak at $\sim$3400 cm^{-1} in the experimental IR spectra of the aqueous mixture of ETH in the intermediate region is due to the contribution of the water–ETH hydrogen bond mainly from the O–H$_{ETH}\cdots$O$_w$ hydrogen bonds as supported also by the MD simulation results.

In contrast to ETH, the most stable as well as populated (30%) structure of the MFE–water complex is a cyclic structure having O–H$_{MFE}\cdots$O$_w$ and O–H$_w\cdots$F$_{MFE}$ interactions (B1). Apart from the linear O–H$_w\cdots$O$_{MFE}$ (B3) and O–H$_{MFE}\cdots$O$_w$ (B4) hydrogen bonded structure, we have also found another cyclic structure where both OH groups of water act as a donor and interact with the MFE *via* O–H$_w\cdots$O$_{MFE}$ and O–H$_w\cdots$F$_{MFE}$ interactions (B2) and its stability and population (20% each) is almost similar to the linear hydrogen bonded structure. The structure having linear O–H$_w\cdots$F$_{MFE}$ interaction (B5) is the least stable and populated. The BCPs for all the interactions of the MFE–water complex are (3, −1) and the values of ρ and ∇^2 are within the range of non-covalent interactions indicating that apart from the O–H$_{MFE}\cdots$O$_w$ and O–H$_w\cdots$O$_{MFE}$ interactions, the O–H$_w\cdots$F$_{MFE}$ interaction is also hydrogen bonded. Moreover, for the structures B1 and B2, (3, +1) ring BCPs have been observed along with two (3, −1) BCPs confirming the cyclic nature of the structure. The ρ and ∇^2 values for the O–H$\cdots$O interaction of the structure B1 is higher as compared to other structures (B2–B4) indicating that O–H$_w\cdots$F$_{MFE}$ interaction of B1 cooperates in the formation of a comparatively strong O–H$_{MFE}\cdots$O$_w$ hydrogen bond which is in line with the MD simulation results.

The O–H stretching for the O–H$_w\cdots$F$_{MFE}$ hydrogen bonded system appears at $\sim$3630 cm^{-1} which is in close agreement with the experimental IR data observed at $\sim$3640 cm^{-1} confirming the presence of O–H$_w\cdots$F$_{MFE}$ interacted species. We have also assured the presence of O–H$_w\cdots$F$_{MFE}$ interacted species by the IR measurements of the C–F stretching frequency supported by the theoretical frequency calculations as well as fluorine NMR data. The C–F stretching frequency calculation data (Table 1) show that the O–H$_w\cdots$F$_{MFE}$ hydrogen bonded complexes show a red shift in their C–F stretching frequency (B1, B2 and B5) whereas a blue shift in the C–F stretching frequency has been observed for the structures in which the C–F group is not directly involved in the hydrogen bonding. The experimental C–F stretching data for the aqueous mixture of MFE shows a red shift in the C–F stretching frequency and ^{19}F NMR exhibits a downfield chemical shift (Fig. S4, ESI†) which affirms the presence of the O–H$_w\cdots$F$_{MFE}$ hydrogen bonded complex in its aqueous mixture. The calculated IR feature for the MFE–water interaction (O–H$_{MFE}\cdots$O$_w$) appears at $\sim$3400 cm^{-1} which also matches with the observed increased intensity of the experimental IR in the water rich as well as intermediate regions of the aqueous mixture of MFE. It is important to mention that the intensity of the experimental IR peak at 3400 cm^{-1} as well as the $\sim$3640 cm^{-1} peak increases simultaneously for the aqueous mixture of MFE in its water rich as well as the intermediate region which clearly indicates that the O–H$_w\cdots$F$_{MFE}$ hydrogen bond cooperates in the formation of O–H$_{MFE}\cdots$O$_w$ hydrogen bonds *via* a cyclic structure, also supported by the MD simulation results. Experimental IR data, MD simulation as well as quantum chemical calculations clearly establish that the fluorination of ETH induces a change in the orientation as well as the hydrogen bonding sites of the water molecule which in turn increases the strength of the O–H$_{MFE}\cdots$O$_w$ hydrogen bond as well as decreases the clustering of water molecules. Indeed, under supersonic jet conditions, it has been found that water forms a cyclic complex having O–H$\cdots$F and O–H$\cdots$O contacts with the fluorinated alcohols.[18,43,53]

Conclusions

The combined experimental as well as theoretical studies show that the addition of a small amount of ETH in pure water increases the aggregation of water more as compared to the hydrogen bonding between the ETH and water molecules. On the other hand, for the aqueous mixture of MFE, water interacts with the fluorine of MFE *via* $O–H_w\cdots F_{MFE}$ interactions which increases the number of $O–H_{MFE}\cdots O_w$ hydrogen bonds as well as decreases the clustering of water molecules. The increased number of alcohol–water hydrogen bonds and decreased clustering of water molecules results in an increase in the intensity of the IR peak at 3370 cm^{-1} more than at 3200 cm^{-1} whereas the appearance of the high frequency peak at $\sim$3640 cm^{-1} signifies the $O–H_w\cdots F_{MFE}$ interaction. The IR study, MD simulation and quantum chemical studies combinedly lead to the conclusion that the substitution of fluorine on ETH, changes the water orientation as well as the interaction sites from the oxygen end to the fluorine of MFE *via* $O–H_w\cdots F_{MFE}$ interactions which cooperate in the formation of more $O–H_{MFE}\cdots O_w$ hydrogen bonds.

Conflicts of interest

There are no conflicts to declare.

Acknowledgements

This work was supported partially by the research grants provided by the Council of Scientific and Industrial Research (CSIR) [Grant No. 01(2803)/14/EMR-II] as well as the Department of Science and Technology (DST-SERB) [Grant No. EMR/2015/001605] India. S. M., B. B., and T. N. thank institute and CSIR for their fellowships, respectively.

References

1 B. Milorey, S. Farrell, S. E. Toal and R. Schweitzer-Stenner, *Chem. Commun.*, 2015, **51**, 16498.
2 S. Jalili and M. Akhavan, *J. Chem. Theory Comput.*, 2009, **08**, 215.
3 M. Fioroni, M. D. Diaz, K. Burger and S. Berger, *J. Am. Chem. Soc.*, 2002, **124**, 7737.
4 N. Prabhu and K. Sharp, *Chem. Rev.*, 2006, **106**, 1616.
5 S. Mondal, R. Halder, B. Biswas, B. Jana and P. C. Singh, *J. Chem. Phys.*, 2016, **144**, 184504.
6 B. Biswas, S. Mondal and P. C. Singh, *ChemistrySelect*, 2016, **1**, 5607.
7 D. Gao, T. Kobayashi and S. Adachi, *J. Appl. Glycosci.*, 2014, **61**, 9.
8 Y. Moroi, H. Takagi, S. Nagadome, Y. Hirata and G. Sugihara, *J. Colloid Interface Sci.*, 1992, **149**, 252.
9 M.-L. Tan, B. T. Miller, J. Te, J. R. Cendagorta, B. R. Brooks and T. Ichiye, *J. Chem. Phys.*, 2015, **142**, 064501.
10 M. Matsugami, R. Yamamoto, T. Kumai, M. Tanaka, T. Umecky and T. Takamuku, *J. Mol. Liq.*, 2016, **217**, 3.
11 G. Guevara-Carrion, J. Vrabec and H. Hasse, *J. Chem. Phys.*, 2011, **134**, 074508.
12 S. Burikov, T. Dolenko, S. Patsaeva, Y. Starokurov and V. Yuzhakov, *Mol. Phys.*, 2010, **108**, 2427.
13 T. Takamuku, K. Saisho, S. Nozawa and T. Yamaguchi, *J. Mol. Liq.*, 2005, **119**, 133.
14 T. A. Scott, *J. Phys. Chem.*, 1946, **50**, 406.
15 B. Biswas, S. Mondal and P. C. Singh, *J. Phys. Chem. A*, 2017, **121**, 1250.
16 R. E. Rosenberg, *J. Phys. Chem. A*, 2016, **120**, 7519.
17 R. A. Cormanich, R. Rittner, M. P. Freitas and M. Bühl, *Phys. Chem. Chem. Phys.*, 2014, **16**, 19212.
18 M. Heger, T. Scharge and M. A. Suhm, *Phys. Chem. Chem. Phys.*, 2013, **15**, 16065.
19 E. Clot, O. Eisenstein, N. Jasim, S. A. Macgregor, J. E. McGrady and R. N. Perutz, *Acc. Chem. Res.*, 2011, **44**, 333.
20 C. N. Neumann and T. Ritter, *Angew. Chem., Int. Ed.*, 2015, **54**, 3216.
21 E. N. G. Marsh, *Acc. Chem. Res.*, 2014, **47**, 2878.
22 Y. Tang, G. Ghirlanda, W. A. Petka, T. Nakajima, W. F. DeGrado and D. A. Tirrell, *Angew. Chem., Int. Ed.*, 2001, **40**, 1494.
23 B. Bilgiçer, A. Fichera and K. Kumar, *J. Am. Chem. Soc.*, 2001, **123**, 4393.
24 T. Takamuku, M. Tanaka, T. Sako, T. Shimomura, K. Fujii, R. Kanzaki and M. Takeuchi, *J. Phys. Chem. B*, 2010, **114**, 4252.
25 C. Chatterjee and J. T. Gerig, *Biopolymers*, 2007, **87**, 115.
26 C. Chatterjee and J. T. Gerig, *Biochemistry*, 2006, **45**, 14665.
27 W.-Q. Deng, V. Molinero and W. A. Goddard, *J. Am. Chem. Soc.*, 2004, **126**, 15644.
28 K.-C. Liao, C. M. Bowers, H. J. Yoon and G. M. Whitesides, *J. Am. Chem. Soc.*, 2015, **137**, 3852.
29 M. D. Schuh and M. C. Baldwin, *J. Phys. Chem. B*, 2006, **110**, 10903.
30 J. F. Parsons, G. Xiao, G. L. Gilliland and R. N. Armstrong, *Biochemistry*, 1998, **37**, 6286.
31 M. Castagnola, L. Cassiano, I. Messana, M. Paci, D. V. Rossetti and B. Giardina, *J. Chromatogr. A*, 1996, **735**, 271.
32 T. Narita, *Polym. J.*, 2011, **43**, 497.
33 K. K. Matsumoto, M. Matsuoka and H. Yamaoka, *Macromolecules*, 1999, **32**, 7122–7127.
34 K. Müller, C. Faeh and F. Diederich, *Science*, 2007, **317**, 1881.
35 H.-J. Böhm, D. Banner, S. Bendels, M. Kansy, B. Kuhn, K. Müller, U. Obst-Sander and M. Stahl, *ChemBioChem*, 2004, **5**, 637.
36 M. E. Evans, C. L. Burke, S. Yaibuathes, E. Clot, O. Eisenstein and W. D. Jones, *J. Am. Chem. Soc.*, 2009, **131**, 13464.
37 Q. Shao, *Proteins*, 2014, **82**, 944.
38 B. C. Buer, J. L. Meagher, J. A. Stuckey and E. N. G. Marsh, *Proc. Natl. Acad. Sci. U. S. A.*, 2012, **109**, 4810.
39 K. Gast, D. Zirwer, M. Müller-Frohne and G. Damaschun, *Protein Sci.*, 1999, **8**, 625.
40 J. Huang and K. Hedberg, *J. Am. Chem. Soc.*, 1989, **111**, 6909.
41 P. Buckley, P. A. Giguère and D. Yamamoto, *Can. J. Chem.*, 1968, **46**, 2917.

42 R. E. Rosenberg, *J. Phys. Chem. A*, 2012, **116**, 10842.
43 T. Scharge, N. Wassermann Tobias and A. Suhm Martin, *Z. Phys. Chem.*, 2008, **222**, 1407.
44 M. J. Abraham, D. van der Spoel, E. Lindahl and B. Hess, and the GROMACS development team, *GROMACS User Manual version 5.1.2*, www.gromacs.org, 2016.
45 S. Canzar, M. El-Kebir, R. Pool, K. Elbassioni, A. K. Malde, A. E. Mark, D. P. Geerke, L. Stougie and G. W. Klau, *J. Comput. Biol.*, 2013, **20**, 188.
46 A. K. Malde, L. Zuo, M. Breeze, M. Stroet, D. Poger, P. C. Nair, C. Oostenbrink and A. E. Mark, *J. Chem. Theory Comput.*, 2011, **7**, 4026.
47 H. J. C. Berendsen, J. P. M. Postma, W. F. v. Gunsteren, A. DiNola and J. R. Haak, *J. Chem. Phys.*, 1984, **81**, 3684.
48 M. Parrinello and A. Rahman, *J. Appl. Phys.*, 1981, **52**, 7182.
49 D. Frenkel and B. Smit, *Understanding Molecular Simulation*, Academic, San Diego, CA, 2nd edn, 2002.
50 M. J. Frisch, G. W. Trucks, H. B. Schlegel, G. E. Scuseria, M. A. Robb, J. R. Cheeseman, G. Scalmani, V. Barone, B. Mennucci, G. A. Petersson, H. Nakatsuji, M. Caricato, X. Li, H. P. Hratchian, A. F. Izmaylov, J. Bloino, G. Zheng, J. L. Sonnenberg, M. Hada, M. Ehara, K. Toyota, R. Fukuda, J. Hasegawa, M. Ishida, T. Nakajima, Y. Honda, O. Kitao, H. Nakai, T. Vreven, J. A. Montgomery, Jr., J. E. Peralta, F. Ogliaro, M. Bearpark, J. J. Heyd, E. Brothers, K. N. Kudin, V. N. Staroverov, T. Keith, R. Kobayashi, J. Normand, K. Raghavachari, A. Rendell, J. C. Burant, S. S. Iyengar, J. Tomasi, M. Cossi, N. Rega, J. M. Millam, M. Klene, J. E. Knox, J. B. Cross, V. Bakken, C. Adamo, J. Jaramillo, R. Gomperts, R. E. Stratmann, O. Yazyev, A. J. Austin, R. Cammi, C. Pomelli, J. W. Ochterski, R. L. Martin, K. Morokuma, V. G. Zakrzewski, G. A. Voth, P. Salvador, J. J. Dannenberg, S. Dapprich, A. D. Daniels, O. Farkas, J. B. Foresman, J. V. Ortiz, J. Cioslowski and D. J. Fox, *Gaussian 09, Revision B.01*, Gaussian, Inc., Wallingford CT, 2009.
51 R. F. W. Bader, *Acc. Chem. Res.*, 1985, **18**, 9.
52 B. Ratajska-Gadomska and W. Gadomski, *J. Chem. Phys.*, 2010, **133**, 234505.
53 T. Scharge, C. Emmeluth, T. Häber and M. A. Suhm, *J. Mol. Struct.*, 2006, **786**, 86.
54 P. C. Singh, K.-I. Inoue, S. Nihonyanagi, S. Yamaguchi and T. Tahara, *Angew. Chem., Int. Ed.*, 2016, **55**, 10621.
55 P. C. Singh, S. Nihonyanagi, S. Yamaguchi and T. Tahara, *J. Chem. Phys.*, 2013, **139**, 161101.
56 G. E. Walrafen, in *Water, A Comprehensive Treatise*, ed. F. Franks, Plenum Press, New York, 1972, vol. 1, ch. 5.
57 B. Ratajska-Gadomska and W. Gadomski, *J. Chem. Phys.*, 2004, **121**, 12583.
58 J. L. Green, A. R. Lacey and M. G. Sceats, *J. Phys. Chem.*, 1986, **90**, 3958.
59 K. M. Murdoch, T. D. Ferris, J. C. Wright and T. C. Farrar, *J. Chem. Phys.*, 2002, **116**, 5717.
60 V. Crupi, S. Interdonato, F. Longo, D. Majolino, P. Migliardo and V. Venuti, *J. Raman Spectrosc.*, 2008, **39**, 244.
61 S. Y. Noskov, G. Lamoureux and B. Roux, *J. Phys. Chem. B*, 2005, **109**, 6705.
62 M. D'Angelo, G. Onori and A. Santucci, *J. Chem. Phys.*, 1994, **100**, 3107.